ACS APPLIED MATERIALS & INTERFACES

Research Article

www.acsami.org

# Fabrication of Tantalum and Nitrogen Codoped ZnO (Ta, N-ZnO) Thin Films Using the Electrospay: Twin Applications as an Excellent Transparent Electrode and a Field Emitter

Khalid Mahmood,[†,‡] Seung Bin Park,*[,†] and Hyung Jin Sung[‡]

[†]Department of Chemical & Biomolecular Engineering and [‡]Department of Mechanical Engineering, Korea Advanced Institute of Science and Technology, 291 Daehak-ro, Yuseong-gu, Daejeon, 305-701, Republic of Korea

**ABSTRACT:** The realization of stable p-type nitrogen-doped ZnO thin films with durable and controlled growth is important for the fabrication of nanoscale electronic and optoelectronic devices. ZnO thin films codoped with tantalum and nitrogen (Ta, N-ZnO) were fabricated by using the electrospraying method at an atmospheric pressure. X-ray diffraction (XRD) studies demonstrated that all the prepared films were polycrystalline in nature with hexagonal wurtzite structure. In addition, a shift in the XRD patterns was observed, and the crystal orientation was changed at a certain amount of nitrogen (>6 at.%) in the starting solution. Analysis of X-ray diffraction patterns and X-ray photoelectron spectra revealed that nitrogen which was combined with the zinc atom (N−Zn) was successfully doped into the ZnO crystal lattice. It was also observed that 2 at.% tantalum and 6 at.% nitrogen (2 at.% Ta and 6 at.% N) were the optimal dopant amounts to achieve the minimum resistivity of about $9.70 \times 10^{-5}$ Ω cm and the maximum transmittance of 98% in the visible region. Consequently, the field-emission characteristics of such a Ta, N-ZnO emitter can exhibit the higher current density of 1.33 mA $cm^{-2}$, larger field-enhancement factor ($\beta$) of 4706, lower turn-on field of 2.6 V $\mu m^{-1}$, and lower threshold field of 3.5 V $\mu m^{-1}$ attributed to the enhanced conductivity and better crystallinity of films. Moreover, the obtained values of resistivity were closest to the lowest resistivity values among the doped ZnO films as well as to the indium tin oxide (ITO) resistivity values that were previously studied. We confirmed that the tantalum and nitrogen atoms substitution in the ZnO lattice induced positive effects in terms of enhancing the free carrier concentration which will further improve the electrical, optical, and field-emission properties. The proposed electrospraying method was well suitable for the fabrication of Ta, N-ZnO thin films at optimum conditions with superior electrical, optical, and field-emission characteristics, implying the potential applications as both a transparent electrode and field-emission (FE) devices.

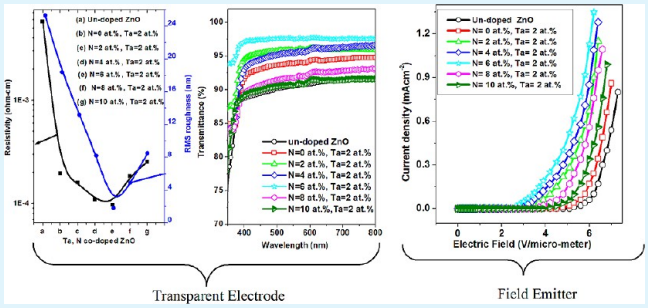


**KEYWORDS:** *Co-doped ZnO thin films, conductivity, optical properties, electrospray, field-emission*

## 1. INTRODUCTION

Zinc oxide (ZnO) has drawn a great deal of attention as a transparent conductive oxide and wide band gap material and has applications in light-emitting devices, UV detectors, flat displays, and solar cells.[1] It also has potential usage in low-voltage field-emission (FE) devices,[2] owing to its high thermal stability,[3] low electron affinity, and high oxidation resistance in harsh environments. Since pure ZnO thin films have inherently poor conductivity, thermal treatment and doping with various dopants are usually necessary to enhance the electrical and optical properties of these films,[4−6] which can also lead to lower turn-on field and higher emission current. For better optoelectronic device fabrication, realization of p-type ZnO films is crucial. High-quality ZnO n-type films can be achieved by subsequent doping with group-III elements (such as Al, Ga, and In) and have already been studied by many researchers.[7−9] It has been reported that group-III doping in ZnO introduces a significant amount of deformation in the lattice structure. Furthermore, Al and In are highly reactive with oxygen, leading to oxidation during film growth. Thus, an alternative doping element is needed to alleviate such problems. Tantalum (Ta) as a dopant is among the good candidates for producing high-quality n-type ZnO thin films owing to its low material toxicity, low cost, suitable ionic radius, and ease of handling. In the case of p-type doping, however, ZnO exhibits high resistance to the formation of shallow acceptor levels because of its asymmetric doping limitations.[10] Theoretically, group-I elements substituting on the Zn site are shallow acceptors, but these dopants tend to occupy interstitial sites, thereby behaving as a donor. In the past, considerable efforts have been made to realize p-type ZnO by N doping.[11,12] Nitrogen (N) is considered as a good p-type dopant in ZnO because of the smallest atomic size and the lowest p-orbital energy among the group-V elements.[13] Recently, several researchers studied the p-type ZnO growth by codoping techniques, such as N−Be by sputtering,[14] N−In doping by spray pyrolysis,[15] N−Al by DC reactive magnetron

Received: January 25, 2013
Accepted: April 2, 2013
Published: April 2, 2013

   dx.doi.org/10.1021/am4003342 | ACS Appl. Mater. Interfaces 2013, 5, 3722−3730

sputtering,[16] and N−Ga by pulsed laser deposition (PLD).[17] However, no report is available on p-type ZnO formation by codoping of nitrogen and tantalum. In addition, in a previous report, we studied the performance of boron- and tantalum-doped ZnO thin films.[18] We reported that 2 at.% tantalum-doped ZnO (TaZO) films have good electrical and optical properties. However, we also concluded that there was no further decrease of electrical resistivity above a certain doping level of tantalum (2 at.%) because the electron scattering effect was caused by the grain boundaries and ionized impurities. There might be less chances of electron scattering if the doping atoms are a substitute for oxygen (O) in the ZnO lattice rather than in the Zn site.[19] Thus, there is an increasing tendency to substitute the oxygen atom with Cl, F, and N atoms. N is approximately equal in size to O atoms, which make it an ideal substitute for O. Excess electrons can be produced by substitution of N into the O site due to one single bond with Zn−N.

Recently, different methods have been used for the preparation of ZnO thin films with varying degrees of sophistication, difficulty of operation, and varying degrees of expenses.[19−23] The electrospraying method is adopted for the preparation of ZnO thin films due to its simple setup, low cost, ease of system parameters, and lower deposition temperature requirements. In this study, undoped ZnO and stable p-type Ta, N-ZnO (Ta = 2 at.%, 0 at.% ≤ $N$ ≤ 10 at.%) thin films were fabricated by the electrospraying method at atmospheric pressure. The effects of N addition on the structural, electrical, optical, and field-emission properties of the TaZO thin films were investigated. Furthermore, an optimal composition of N content was also obtained to get the excellent electrical, optical, and field-emission characteristics. Such investigations of codoped ZnO thin films have great technological implications and would also contribute to fundamental studies. To the best of our knowledge, no work has been reported to date that is relevant to p-type Ta, N-ZnO thin films which can serve as both a transparent electrode and field-emission (FE) devices.

## 2. EXPERIMENTAL DETAILS

**2.1. Deposition of Undoped ZnO and Ta, N-ZnO Thin Films.** Undoped ZnO and Ta, N-ZnO thin films were deposited by using the electrospraying method.[24] The precursors zinc acetate dihydrate, ammonium acetate, and tantalum (v) chloride were dissolved in an ethanol−water (30:70 v/v) mixture to produce a 0.05 M solution. The atomic percentage of the tantalum dopant in the solution was [Ta/Zn] = 2 at.%. The doping level of N was varied between 0 and 10 at.% in the starting solution. A syringe pump (KD200, KD Scientific Inc., U.S.A.) was used to feed the precursor solution to a small needle. The voltage, flow rate, and nozzle to substrate distance were 5.6 kV, 0.003 mL/min, and 4 cm, respectively. The silicon samples of 2 × 2 $cm^2$ dimensions were cut from the wafer and washed by alcohol and acetone in an ultrasonic bath for half an hour, respectively, and used as a substrate. Precursor solution was sprayed for 1 h in all cases, and the source temperature was maintained at 250 °C followed by annealing at 410 °C in air for 1 h.

**2.2. Thin-Film Characterization and Property Measurements.** For the surface morphology of the films, scanning electron microscopy (SEM) was performed using a Nova 320 and Magellan 400 microscope coupled with an X-ray energy-dispersive spectrometer (DX-4), for elementary composition of the nanostructures. The crystal structure of the thin films was identified through a D8 DISCOVER X-ray diffractometer using Cu K$\alpha$ radiation ($\lambda$ = 1.5405 Å). The X-ray photoelectron spectra (XPS) of each sample were identified by X-ray photoelectron spectroscopy (Thermo VG Scientific, Sigma Probe). The surface roughness was examined by using a commercial atomic force microscope (AFM) (SPA 400, SII). A UV−visible spectrometer (UV-3101PC) was used to measure the optical transmittance. Electrical resistivity, carrier concentration, and Hall mobility were measured by Hall effect measurement (HMS-3000). Field-emission measurements were performed in a homemade vacuum chamber with a pressure lower than 6 × $10^{-7}$ Pa at room temperature under a two-parallel-plate configuration. The samples were connected to the cathode, whereas another parallel stainless-steel plate worked as the anode. The distance between the anode and cathode was kept at about 200 $\mu$m. For the degassing of samples and the removal of contaminates, a high voltage of ∼4 kV was applied. After that a voltage with a sweep step of 50 V was applied between the cathode and anode to supply an electric field $E$. The emission current was monitored by a Keithley 485 picoammeter.

## 3. RESULTS AND DISCUSSION

**3.1. Microstructure and Compositional Analysis of Undoped ZnO and Ta, N-ZnO Thin Films.** Figure 1 shows

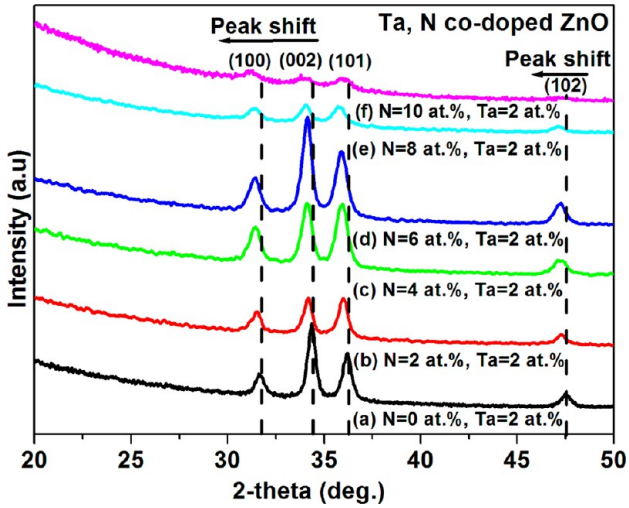


**Figure 1.** XRD patterns of Ta, N-ZnO (Ta = 2 at.%, 0 at.% ≤ $N$ ≤ 10 at.%) thin films.

the X-ray diffraction (XRD) patterns of the Ta, N-ZnO (Ta = 2 at.%, 0 at.% ≤ N ≤ 10 at.%) thin films. All the samples were polycrystalline in nature and showed the single-phase ZnO hexagonal wurtzite structure.[25] Moreover, the preferential $c$-axis orientation of all films was found to be along the (0 0 2) crystal plane caused by the effects of substrate, deposition conditions, and thermal treatments.[26,27] In addition, a small shift (denoted by dashed lines) to lower diffraction angles was examined due to the substitution of a larger radius $N^{3-}$ (146 pm), with a smaller radii $O^{2-}$ (140 pm).[28] The reflected intensity at the (0 0 2) plane appeared to increase as the N content was increased. A strong (0 0 2) diffraction peak in ZnO indicated that the films have a preferred orientation with the $c$-axis normal to the glass substrate.[29] The XRD results suggested that the addition of nitrogen has an effect on the crystallites due to the crystal distortion by substitution of larger ionic radius fluorine (146 pm), which hinders the growth of ZnO along the $c$-direction since it was previously reported that the distortion of the lattice and some lattice defects were observed when the dopant atoms of different sizes were substituted in the ZnO lattice.[30] Other studies also explained that the ZnO film was less oriented along the $c$-axis when it was doped with gallium.[31] Moreover, such preferred basal orientation along the (0 0 2) crystal plane was typically observed in the previously reported Al-doped ZnO

**Table 1. Effect of Nitrogen Incorporation on the Lattice Parameters and Grain Size of Tantalum-Doped ZnO Thin Films**

| film type | *a*-axis (nm) | *c*-axis (nm) | grain size (nm) |
|---|---|---|---|
| undoped ZnO | 0.3270 ± 0.0004 | 0.5230 ± 0.0004 | 37.9 ± 1.5 |
| N = 0 at.%, Ta = 2 at.% | 0.3268 ± 0.0004 | 0.5229 ± 0.0004 | 30.8 ± 1.3 |
| N = 2 at.%, Ta = 2 at.% | 0.3267 ± 0.0004 | 0.5228 ± 0.0004 | 27.5 ± 1.5 |
| N = 4 at.%, Ta = 2 at.% | 0.3264 ± 0.0003 | 0.5226 ± 0.0004 | 25.3 ± 1.4 |
| N = 6 at.%, Ta = 2 at.% | 0.3260 ± 0.0004 | 0.5222 ± 0.0004 | 18.2 ± 1.5 |
| N = 8 at.%, Ta = 2 at.% | 0.3259 ± 0.0005 | 0.5221 ± 0.0004 | 17.4 ± 1.4 |
| N = 10 at.%, Ta = 2 at.% | 0.3258 ± 0.0004 | 0.5220 ± 0.0004 | 16.3 ± 1.5 |

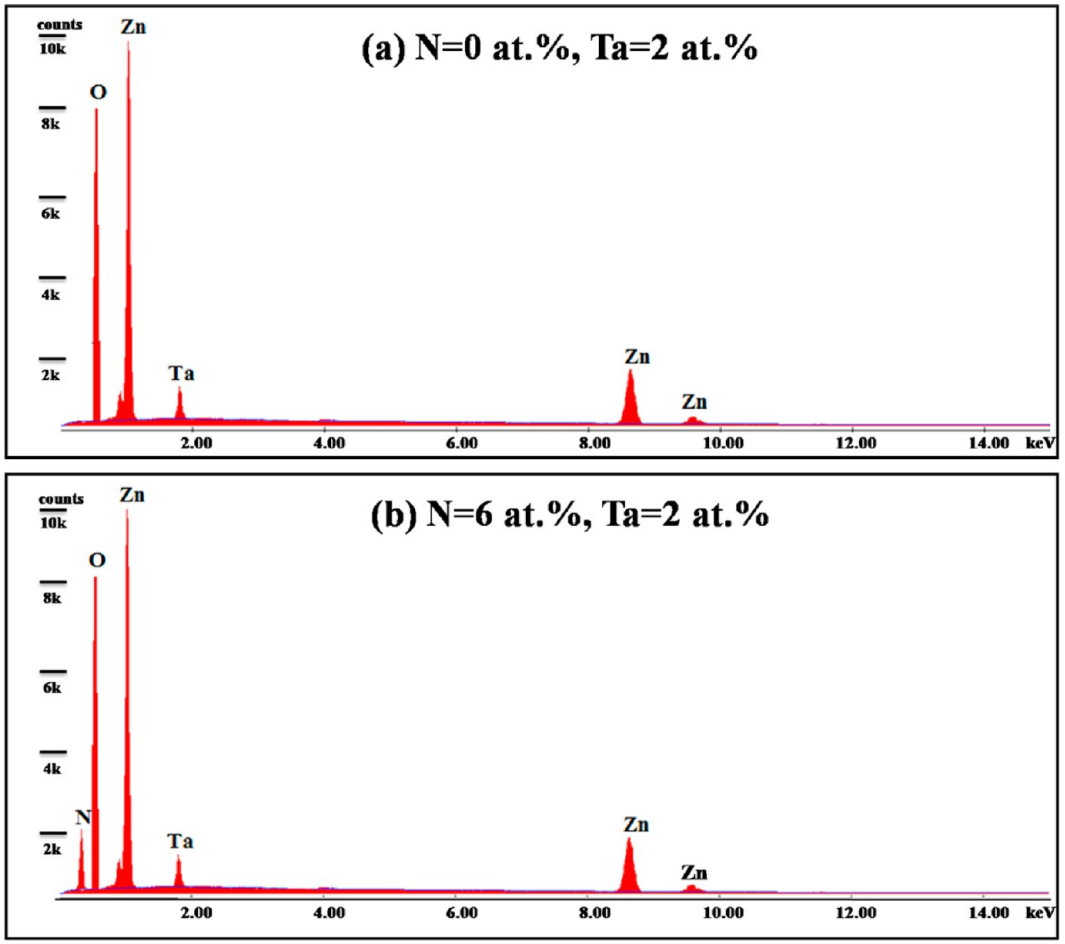


**Figure 2.** Typical EDX patterns of (a) N = 0 at.%, Ta = 2 at.% and (b) N = 6 at.%, Ta = 2 at.% codoped ZnO thin films, respectively.

films for doping range of 1−4 at.% and 1−5 at.%, respectively, at the substrate temperature of 450 °C.[32,33] Furthermore, our results agreed well with previously reported studies.[34−36]

We also investigated the effect of incorporating N atoms by estimating the grain sizes with the help of the Scherrer equation, to the full width at half-maximum of the (0 0 2) reflection of thin films. The estimation of grain size was expressed as follows[37]

$$D = 0.9\lambda/\beta \cos\theta \quad (1)$$

where $\lambda$ is the X-ray wavelength; $\theta$ is the Bragg diffraction angle; and $\beta$ is the full width at half-maximum (FWHM). The grain size (Table 1) decreased from 37.9 to 16.3 nm as the N contents were increased in the solution. This can be due to interference with the aggregation of grains. This trend suggested that N atoms create new nucleation centers in the vacancy of ZnO sites, which will destroy the crystalline structure at high doping level. The decrease in the grain size was also correlated with the broadening of the XRD peak. The lattice parameters, *a* (the second nearest-neighbor distance) and *c* (the length of the bond parallel to the *c*-axis), calculated from the XRD patterns are also presented in Table 1. Compared with undoped ZnO film, the *a*-axis lattice parameter became smaller from 0.3270 nm (ZnO) to 0.3258 nm (2 at.% Ta and 10 at.% N codoped ZnO) thin films. The *c*-axis lattice parameter was also decreased from 0.5230 to 0.5220 nm accordingly, due to the substitution of a larger radius $N^{3-}$ (146 pm), with a smaller radii $O^{2-}$ (140 pm). The decrease in grain size and the lattice parameters as a function of N contents are shown in Table 1.

The typical EDX patterns for the 2 at.% Ta and 0 at.% N codoped ZnO and as well as for 2 at.% Ta and 6 at.% N codoped ZnO thin films were shown in Figure 2a and 2b, respectively. Figure 2a showed only the presence of Ta, Zn, and

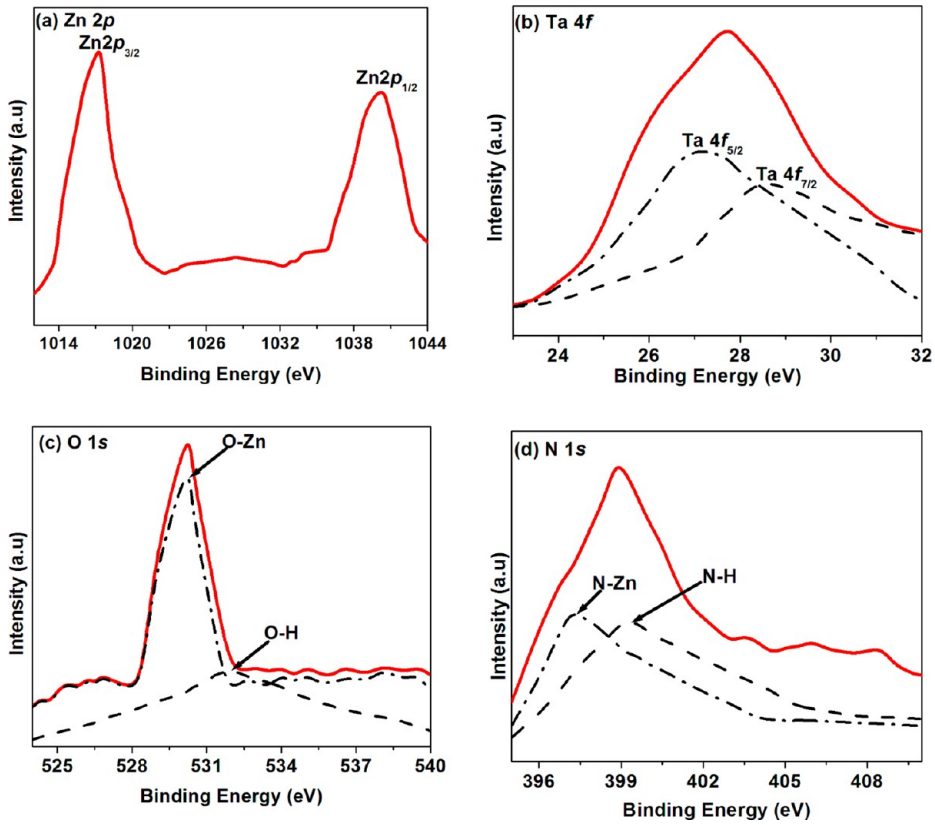


**Figure 3.** XPS spectra for 2 at.% Ta and 6 at.% N codoped ZnO thin films: (a) Zn $2p_{3/2}$ XPS spectrum, (b) Ta 4f XPS spectrum, (c) O 1s XPS spectrum, and (d) N 1s XPS spectrum.

O in the 2 at.% TaZO thin films with no N content. On the other hand, Figure 2b exhibited the energy-dispersive spectroscopy (EDS) measurement of 2 at.% Ta and 6 at.% N codoped ZnO films, which revealed the coexistence of Ta, N, Zn, and O in Ta, N-ZnO thin films, demonstrating that tantalum and nitrogen atoms have been successfully doped into the ZnO thin films. In addition, by scanning 2 at.% Ta and 6 at.% N codoped ZnO thin films in different areas, the average N concentration was estimated to be ~5.9 at.%, which proved that the average amount of N was approximately 5.9 at.% throughout the film.

To obtain more accurate information, we used X-ray photoelectron spectroscopy (XPS) to examine the chemical bonding of the 2 at.% Ta and 6 at.% N codoped ZnO thin films, as shown in Figure 3. The XPS spectra have been charge corrected to the adventitious C 1s peak at 284.2 eV, and the core states of Zn 2p, Ta 4f, O 1s, and N 1s peaks were also observed. Figure 3a shows the two peaks at 1017.22 and 1040.20 eV corresponding to Zn $2p_{3/2}$ and Zn $2p_{1/2}$. The energy difference between two Zn 2p peaks was 22.98 eV, which agreed well with the standard value of 22.97.[38] The Ta 4f XPS peak (Figure 3b) was deconvoluted into two subpeaks. The two peaks were located at 28.8 and 26.9 eV with energy separation of 1.9 eV for the Ta $4f_{5/2}$ and Ta $4f_{7/2}$ state, respectively. The Ta 4f peaks shift 0.6 eV toward higher binding energy (BE), attributed to the increasing oxygen content of the tantalum oxide. The Ta $4f_{7/2}$ peak position at 26.9 eV was typical of the $Ta^{5+}$ chemical state in $Ta_2O_5$.[39] The O 1s state splits into two peaks as shown in Figure 3(c). The peak at 530.3 eV can be attributed to the O−Zn bond formation, while the peak at 532.0 eV can be due to the O−H bond formation. In addition, The N 1s peak also consisted of two components, as shown in Figure 3(d). At 397.2 eV, a chemical shift in comparison with the N 1s peak for free amine (399.2 eV) was obtained, which demonstrated the formation of N−Zn bonds. Hence, XPS analysis proves the successful addition of nitrogen into TaZO films.

Figure 4 exhibits the surface morphologies of undoped ZnO and Ta, N-ZnO (Ta = 2 at.%, 0 at.% ≤ N ≤ 10 at.%) thin films. The grain size of the Ta, N-ZnO thin films was gradually decreased as the N contents were increased in the solution. The observed changes in the morphology indicate that N acts as nucleation centers in the vacancy sites of ZnO, which in turn would change the nucleation type from homogeneous to heterogeneous and destroy the crystalline structure at high doping level. It was also possible that the substituted N provided a retarding force within the wurtzite structure opposing the driving force of grain growth, and the grain growth was subsequently inhibited. Generally, an increase in N concentration will enhance the nucleation of the ZnO phase and consequently result in the smaller crystallites. However, it was also examined that, above a certain doping level (>6 at.%) of N, defects such as empty holes were also observed on the surface of films due to the stress of the crystal structure by the substitution of a larger $N^{3-}$ ion (146 pm) as shown in Figure 4f and 4g, respectively. The results agreed well with XRD patterns.

Figure 5a exhibits the surface roughness and electrical resistivity data for undoped ZnO and Ta, N-ZnO (Ta = 2 at.%, 0 at.% ≤ N ≤ 10 at.%) thin films. The results showed that the addition of N atoms has an influence on the grain size and surface roughness of the films. It was also examined that when N was added to the TaZO (2 at.%) thin films a significant


dx.doi.org/10.1021/am4003342 | ACS Appl. Mater. Interfaces 2013, 5, 3722−3730

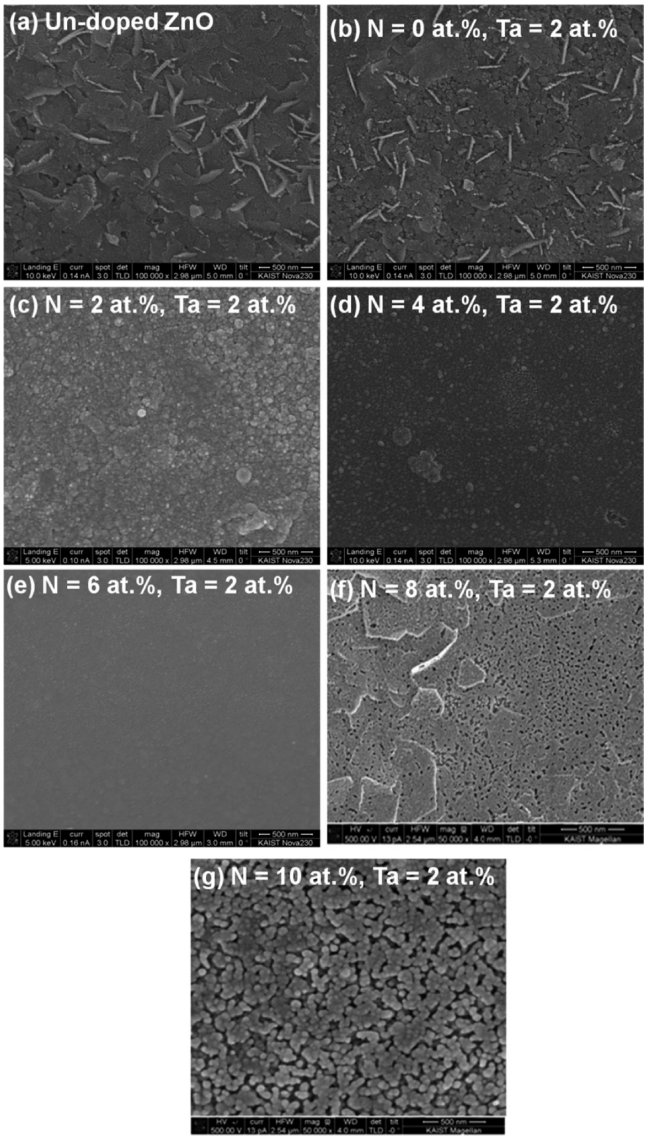


**Figure 4.** FE-SEM images of undoped ZnO and Ta, N−ZnO (Ta = 2 at.%, 0 at.% ≤ N ≤ 10 at.%) thin films.

decrease in surface roughness less than that of undoped ZnO films was observed. The decrease in roughness can be attributed to the reduction in grain size with more compact and uniform surface morphology as evident from SEM images in Figure 4. In addition, the surface roughness approaches to attain the smallest value of 1.9 nm, and a very fine thin film was obtained when the N content was 6 at.% in the solution. This film also exhibited the minimum resistivity of order of 9.70 × $10^{-5}$ Ω cm. Furthermore, our results agreed well with previously reported studies.[35,36] Figure 5b exhibits the cross-sectional SEM and 2 $\mu$m × 2 $\mu$m sized AFM images for undoped ZnO as well as 2 at.% Ta and 6 at.% N codoped ZnO films. Film thickness was measured from the cross-sectional SEM images (Figure 5b), and it was found that all the films have the same thickness of about 150 ± 10 nm. The AFM images (Figure 5b) also revealed that the homogeneous ZnO and Ta, N-ZnO films across the entire surface which was grown by the electrospraying method and annealing resulted in a relatively flat surface. From the results of XRD, XPS, EDS, SEM, and AFM analysis, it has been justified that N atoms are substituted into the ZnO lattice which forms Zn−N chemical

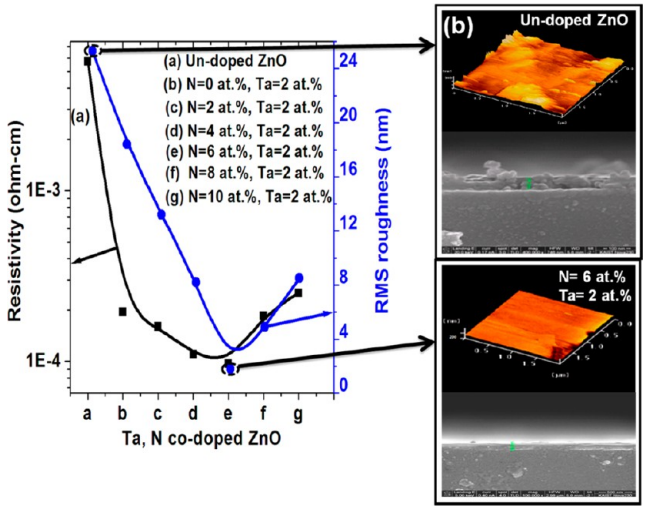


**Figure 5.** (a) Electrical resistivities and surface roughness data of undoped ZnO and Ta, N−ZnO (Ta = 2 at.%, 0 at.% ≤ N ≤ 10 at.%) films and (b) atomic force microscopy (AFM) images and cross-sectional SEM images for undoped ZnO and Ta = 2 at.%, N = 6 at.% codoped ZnO films, respectively.

bonding, with smoother and denser film surface. However, when the N contents are more than 6 at.%, stress was caused by lattice mismatch, and empty holes on the film surface were generated.

**3.2. Optical and Electrical Properties of Undoped ZnO and Ta, N-ZnO Thin Films.** Figure 6a shows the optical

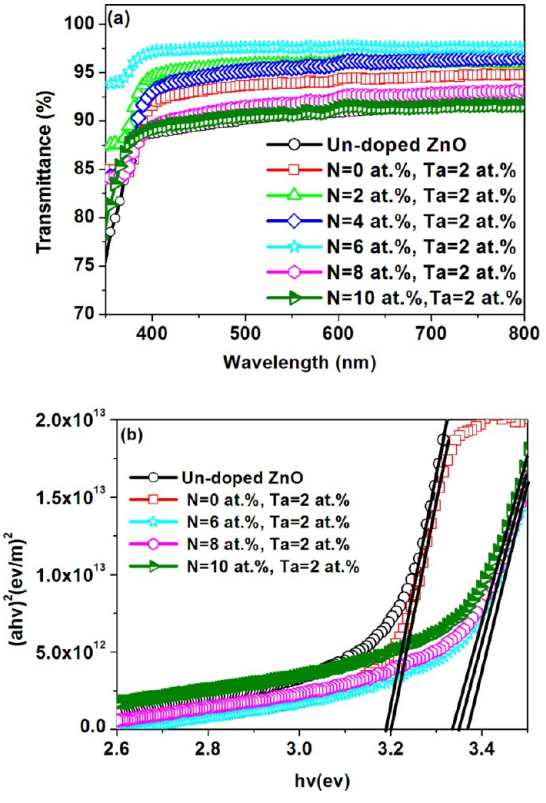


**Figure 6.** (a) Optical transmission spectra of the undoped ZnO and Ta, N−ZnO (Ta = 2 at.%, 0 at.% ≤ N ≤ 10 at.%) thin films and (b) the optical band gap of the undoped ZnO and Ta, N−ZnO films, respectively.


dx.doi.org/10.1021/am4003342 | ACS Appl. Mater. Interfaces 2013, 5, 3722−3730

**Table 2. Variation of Resistivity, Carrier Concentration, and Mobility for Undoped ZnO and Ta, N−ZnO (Ta = 2 at.%, 0 at.% ≤ N ≤ 10 at.%) Thin Films**

| film type | resistivity [$10^{-4}$ Ω cm] | carrier concentration [$10^{21}$ $cm^{-3}$] | mobility [$cm^2$ $(V\ s)^{-1}$] |
|---|---|---|---|
| undoped ZnO | 57.5 ± 0.2 | 0.0286 ± 0.0002 | 38.0 ± 2 |
| N = 0 at.%, Ta = 2 at.% | 1.95 ± 0.03 | 0.998 ± 0.001 | 32.1 ± 1 |
| N = 2 at.%, Ta = 2 at.% | 1.60 ± 0.01 | 1.28 ± 0.02 | 30.5 ± 2 |
| N = 4 at.%, Ta = 2 at.% | 1.10 ± 0.02 | 1.98 ± 0.01 | 28.3 ± 2 |
| **N = 6 at.%, Ta = 2 at.%** | **0.97 ± 0.01** | **2.55 ± 0.02** | **25.2 ± 1** |
| N = 8 at.%, Ta = 2 at.% | 1.85 ± 0.02 | 1.58 ± 0.02 | 21.4 ± 2 |
| N = 10 at.%, Ta = 2 at.% | 2.52 ± 0.02 | 1.29 ± 0.02 | 19.2 ± 2 |

transmittance of undoped ZnO and Ta, N-ZnO (Ta = 2 at.%, 0 at.% ≤ N ≤ 10 at.%) thin films. The optical transmittance of all the films stayed greater than 87% for the entire visible range, and the absorption edge for Ta, N codoped ZnO films was shifted to higher levels than those of undoped ZnO films. In our previous report,[18] it was examined that 2 at.% TaZO films showed the optical transmittance greater than 93% for the entire visible range. However, in the present work, the 2 at.% Ta and 6 at.% N codoped ZnO thin films showed the enhancement in optical transmittance (>98%). At a higher concentration of N content, the transmittance decreases may be due to the increased optical scattering of photons caused by the crystal defects which were produced by doping.[40] In addition, when N doping concentration was increased, the absorption edges were shifted toward the shorter wavelength due to the Burstein−Moss shift,[41] as a result of increase in carrier concentration. Moreover, the free carrier absorption of the photons might contribute to the optical transmittance reduction for the heavily doped films. Ta, N-ZnO films deposited by electrospraying indicate a higher transmittance than the boron-doped ZnO (BZO) films and boron and fluorine codoped ZnO (B, F-ZnO) films deposited by other methods such as liquid source misted chemical vapor deposition (LSMCD) and RF magnetron sputtering.[35,36,42] The optical transmittances were above 75% in the short wavelength region, suggesting that the absorption in the UV region significantly depends on the sample structure and also that the ZnO nanoparticles strongly absorb the incident light. As a result of the band-to-band absorption, the light propagating through the sample containing ZnO nanoparticles rapidly decreases, screening the effect of photonic band gap in the transmittance spectrum.[43]

Figure 6b shows the direct optical band gap of undoped ZnO and Ta, N-ZnO thin films. It was examined that the increase in N doping concentration will shift the absorption edge to the higher-energy region of 3.18−3.38 eV. The broadening effect in the band gap might be due to the Burstein−Moss effect,[42,7] which is attributed to the additional free electrons (which occupy the energy states located above the conduction band minimum and fill the band resulting in widening the optical band gap). The shift of band gap seen in Figure 6b can be ascribed to the changes in the crystallite size and lattice parameters. For ZnO films, other reports have also proven that crystallite size affects the optical properties, showing higher band gap energy for films with smaller crystallite size.[44,45] Such a trend was generally observed in the present samples because the crystallite size decreased at higher doping level, hence the higher band gap energy was found. The results agreed well with the study performed on other BZO and B, F-ZnO films, where the band gap was found to increase by increasing the doping level.[35,36]

Table 2 shows the electrical properties of undoped ZnO and Ta, N-ZnO (Ta = 2 at.%, 0 at.% ≤ N ≤ 10 at.%) thin films. In our previous report, it was examined that the minimum value of resistivity was 1.95 × $10^{-4}$ Ω cm for 2 at.% TaZO film.[18] However, it was also examined that there was no further decrease of electrical resistivity above a certain doping level of tantalum (2 at.%) because of the electron scattering effect caused by the ionized impurities and grain boundaries. However, in the present study, it is noticeable that the resistivity decreases more than the above value of (1.95 × $10^{-4}$ Ω cm) to a minimum value of 9.70 × $10^{-5}$ Ω cm when it was codoped with N having a doping concentration of 6 at.%. When the amount of N was increased in the starting solution up to 6 at.%, the resistivity was decreased due to the increase of free carrier concentration. However, after reaching a minimum value, it gradually increases with the further increase in dopant contents because the excess of N doping results in a decrease of carrier concentration which causes again the resistivity to increase. Thus, more than 50% enhancement in the conductivity was achieved when it was codoped with 6 at.% N. It was remarkable that the obtained minimal resistivity values of the order of $10^{-4}$ of Ta, N-ZnO films were comparable at a state-of-the-art level.[46] Furthermore, such lower electrical resistivity values were much better than the resistivity values of other BZO films prepared by the liquid source misted chemical vapor deposition (LSMCD), RF magnetron sputtering,[35,42] and those of Al-doped ZnO thin films by spray pyrolysis and facing targets sputtering.[47,48] Table 2 also shows the values of carrier concentration and Hall mobility of undoped ZnO and Ta, N-ZnO (Ta = 2 at.%, 0 at.% ≤ N ≤ 10 at.%) thin films. It was examined that the Hall mobility decreases when the amount of N increases in the starting solution. This may be due to the decrease of the grain size of the films. However, the carrier concentration increases with the addition of N, which may be due to substitution of N into the O sites. The carrier concentration increases up to 2 at. % Ta and 6 at.% N codoped ZnO films. Further, addition of dopant contents decreases the carrier concentration because the crystal structure becomes disordered.

Figure 7 exhibits the observed values of the optical band gap ($E_g$), plotted against the carrier density ($n$) for the undoped ZnO and Ta, N-ZnO (Ta = 2 at.%, 0 at.% ≤ N ≤ 10 at.%) thin films. The optical band gap energy increases as the carrier concentration increases, until nitrogen content reaches up to 6 at.% in precursor solution. The fitting curve was in good agreement with the Burstein−Moss model.[49] These effects belong to the heavy doped n-type semiconductor: specifically, the Fermi level was inside the conduction band, and the states near the bottom of the conduction band were filled. Free elections enhance the conductivity, and whenever an oxygen

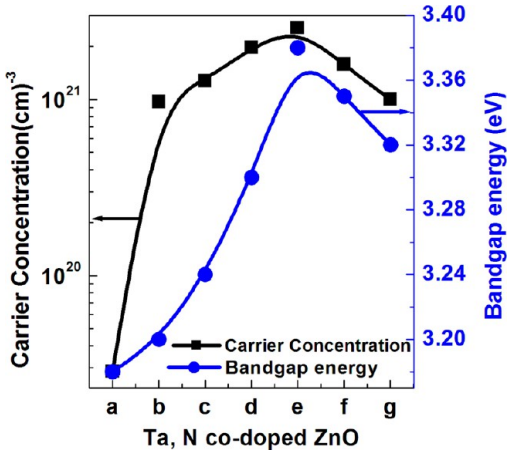


**Figure 7.** Carrier concentration and band gap energy as a function of nitrogen content for undoped ZnO and Ta, N–ZnO (Ta = 2 at.%, 0 at.% ≤ N ≤ 10 at.%): (a) undoped ZnO, (b) N = 0 at.%, Ta = 2 at.%, (c) N = 2 at.%, Ta = 2 at.%, (d) N = 4 at.%, Ta = 2 at.%, (e) N = 6 at.%, Ta = 2 at.%, (f) N = 8 at.%, Ta = 2 at.%, and (g) N = 10 at.%, Ta = 2 at.%, respectively.

site was substituted with a nitrogen atom, the free electrons were artificially created as an oxygen loss.[36]

**3.3. Field-Emission Properties of Undoped ZnO and Ta, N-ZnO Thin Films.** Figure 8a shows the current–field ($J$–$E$) plots of undoped ZnO and Ta, N–ZnO (Ta = 2 at.%, 0 at.% ≤ N ≤ 10 at.%) thin films. The turn-on fields (defined as the $E$ corresponding to the $J$ of 0.01 mA cm$^{-2}$) were about 5.3, 4.8, 3.4, 3.0, 2.6, 3.7, and 4.6 V$\mu$m$^{-1}$ with respect to undoped ZnO and at different N doping concentration of 0 at.% to 10 at.% with a constant tantalum doping concentration of 2 at.%, respectively. The threshold fields (defined as the $E$ where $J$ arrives at 0.1 mA cm$^{-2}$) were about 6.2, 5.8, 4.2, 3.8, 3.5, 4.8, and 5.3 V $\mu$m$^{-1}$ correspondingly. In addition, the corresponding current densities were about 0.10, 0.23, 0.90, 1.10, 1.33, 0.78, and 0.43 mA cm$^{-2}$ under the same electric field of 6.2 V $\mu$m$^{-1}$. It was evident from these results that the field-emission properties of the TaZO thin films were considerably improved after codoping with N in a sense of much lower turn-on and threshold fields compared to that of the undoped ZnO films. In addition, it can be clearly observed that the current density has been significantly increased from 0.10 to 1.33 mA cm$^{-2}$ under the same electric field of 6.3 V $\mu$m$^{-1}$ for an undoped ZnO and 2 at.% Ta and 6 at.% N codoped ZnO thin films, respectively. Such a significant FE performance of codoped ZnO thin films with tantalum and N was attributed to the N dopant because N will provide more electrons in the conduction band of thin films as discussed in the optical performance. The FE performance was in good agreement with the optical and electrical results. The thin films showed the steady emission current for each sample, and also the $J$–$E$ curves have been measured more than 15 times and found to be excellently reproducible.

Furthermore, the FE curves of undoped ZnO and Ta, N–ZnO (Ta = 2 at.%, 0 at.% ≤ N ≤ 10 at.%) thin film devices can be modeled by the Fowler–Nordheim (FN) equation expressed as[50]

$$J = A\left(\frac{\beta^2 E^2}{\Phi}\right)\exp\left(\frac{-B\Phi^{3/2}}{\beta E}\right) \quad (2)$$

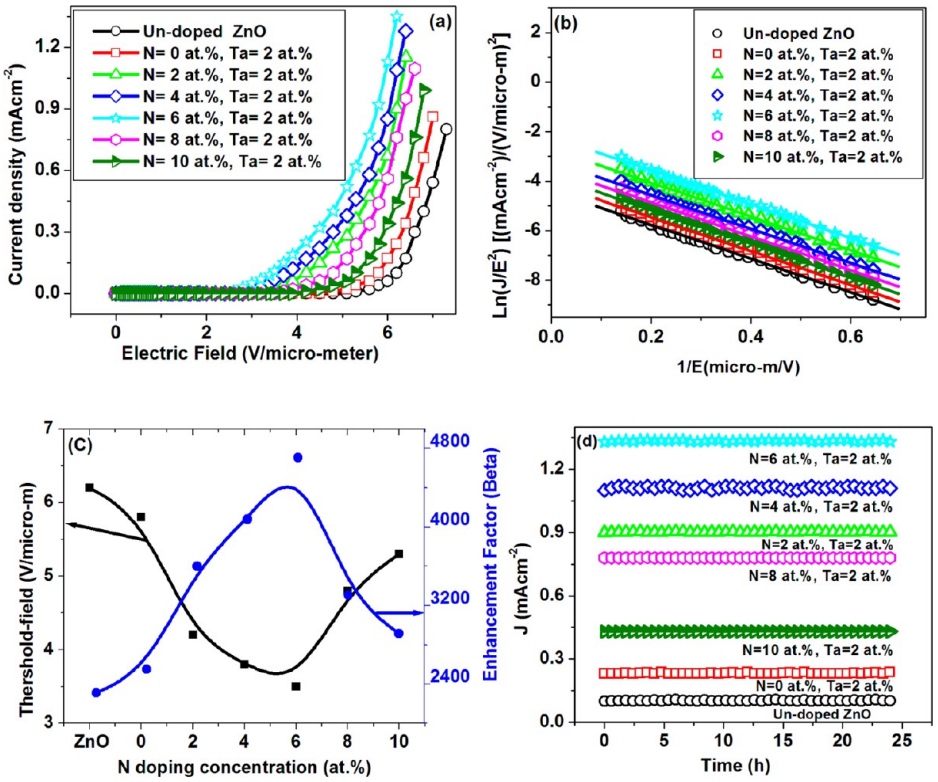


**Figure 8.** (a) $J$–$E$ plot comparison of undoped ZnO and Ta, N–ZnO (Ta = 2 at.%, 0 at.% ≤ N ≤ 10 at.%) thin films; (b) FN plots of the corresponding $J$–$E$ curves; (c) threshold fields and the enhancement factor ($\beta$) as a function of N doping concentration; and (d) emission current density as a function of time demonstrates the long-period field-emission stability.


dx.doi.org/10.1021/am4003342 | ACS Appl. Mater. Interfaces 2013, 5, 3722–3730

where $A = 1.54 \times 10^{-10}$ (A $V^{-2}$ eV), $B = 6.83 \times 10^{9}$ (V $m^{-1}$ $eV^{-3/2}$), and $\Phi$ is the work function, which is about 5.4 eV for ZnO.[51] $\beta$ is the field-enhancement factor, which reflects the ability of the emitters to enhance the local electric field and can be calculated from the FN plot. In addition, the field-enhancement factor was known to depend on several factors, such as geometry of crystal structure, the material conductivity, density of the nanostructures, and the work function.

Figure 8b shows the linear dependence of the corresponding $\ln(J/E^2)$ vs $E^{-1}$(FN) plots of undoped ZnO and Ta, N-ZnO (Ta = 2 at.%, 0 at.% $\leq$ N $\leq$ 10 at.%) thin films with different slopes, indicating the field-emission process from them is a barrier tunneling, quantum mechanical process. According to the FN theory, the slope of the FN plot is equal to $-B\Phi^{3/2}\beta^{-1}$. The slopes obtained from the FN plots can be used to estimate the $\beta$ value. A number of experiments were performed to ensure the stability and reproducibility. The $\beta$ for undoped ZnO and codoped films of tantalum and N were extracted as approximately 2310 $\pm$ 3, 2550 $\pm$ 3, 3599 $\pm$ 3, 4080 $\pm$ 3, 4706 $\pm$ 3, 3307 $\pm$ 3, and 2915 $\pm$ 3, while the N doping concentrations were varied from 0 at.% to 10 at.%, with a constant tantalum doping concentration of 2 at.%, respectively.

Figure 8c exhibits the plots of threshold fields and $\beta$ with respect to undoped ZnO and different N doping concentrations of 0 at.% to 10 at.% with a constant tantalum doping concentration of 2 at.%, respectively. The 2 at.% Ta and 6 at.% N codoped ZnO thin films showed the relatively low threshold field of 3.5 V $\mu m^{-1}$, and the calculated $\beta$ value of 4706 $\pm$ 3 was higher than for the other samples. In addition, the experimental FE characteristics can be connected and consistent with the addressed observations of physical analysis. Generally, a fine nanostructure is critical for the development of field emission devices since it enhances the $\beta$,[52,53] which reflects the ability of emitters to enhance the local electric field. In addition, the less structural defects and superior crystallinity can restrict the carrier trapping and grain boundaries scattering, which can profit carrier lifetime and lead to an advantage of conductivity due to the increases of carrier concentration and mobility.[54,55] Therefore, while the N doping concentration was about 6 at.%, the enhanced FE properties (i.e., the relatively higher $\beta$ value, higher current density, smaller turn-on field, and threshold fields) were probably attributed to the higher conductivity and better crystallinity, which facilitate the electron flow to the emitting surface.[56] Consequently, as the N doping concentration was increased above 6 at.%, the turn-on fields and threshold fields were increased significantly due to the polycrystalline and disorder crystal structure. It indicates that the tantalum and N codoped device with N doping concentration of 6 at.% demonstrates the optimum FE characteristics in this work (i.e., the higher current density of 1.33 mA $cm^{-2}$, larger $\beta$ of ~4706 $\pm$ 3, lower turn-on field of 2.6 V $\mu m^{-1}$, and lower threshold field of 3.5 V $\mu m^{-1}$), due to the superior crystallinity, less structural defects, and better conductivity. In addition, the highest average value of $\beta$ and the lower turn-on and threshold fields can also result from nanometric features and the densely packed 2 at.% Ta and 6 at.% N codoped ZnO thin films which could easily induce much more electron emission than the other films.

The long period emission current stability of undoped ZnO and Ta, N-ZnO (Ta = 2 at.%, 0 at.% $\leq$ N $\leq$ 10 at.%) thin films was also tested by measuring current density, under a constant electric field of 6.2 V $\mu m^{-1}$ as shown in Figure 8d. It can be seen that no obvious degradation of FE current density was observed. The emission current fluctuation was about 5 and 6% during the 25 h, with keeping constant current density about 1.33 and 0.10 mA $cm^{-2}$ for an undoped and 2 at.% Ta and 6 at.% N codoped ZnO thin films, respectively. On the other hand, the constant current densities of about 0.23, 0.90, 1.10, 0.78, and 0.43 mA $cm^{-2}$, respectively, were also shown by other thin films with different nitrogen compositions during 25 h.

These results show the excellent long period emission current stability of the Ta, N-ZnO thin films, which make them highly valuable for practical applications as field emitters. Thus, the overall FE performance of these films deposited by the electrospraying methods at atmospheric pressure, such as turn-on and threshold fields and $\beta$ factor, was excellent compared to that of undoped ZnO and TaZO samples because of the morphology, better crystalline quality, and N-doping ability. Moreover, field emitter devices employing Ta, N-ZnO thin films with advanced field-emission characteristics can also be a best candidate for the applications in flexible field-emission displays.

## 4. CONCLUSIONS

We have investigated the structural, electrical, optical, and field-emission characteristics of undoped ZnO and Ta, N-ZnO (Ta = 2 at.%, 0 at.% $\leq$ N $\leq$ 10 at.%) thin films deposited by the electrospraying method at an atmospheric pressure. XRD studies have shown that the Ta, N codoped ZnO films were polycrystalline in nature. The result of X-ray patterns, XPS, EDS, SEM analysis, and optical experiment exhibited that tantalum and nitrogen atoms were successfully substituted. Moreover, (1 0 2), (0 0 2), (101), and (1 0 2) peaks were shifted toward the smaller-angle direction which was contributed by substitution of N ions. X-ray photoelectron spectroscopy analysis demonstrated that nitrogen and zinc ions combined to a F−Zn bond which could generate an extra electron from the crystal structure. As a result, electrical conductivity was increased due to increased free electron. The tantalum and N atoms substitution into the ZnO lattice has positive effects in terms of enhancing the free electron density and crystallinity of the thin film and hence improvement in electrical, optical, and field-emission properties. The increase of N doping concentration results in smaller grain sizes reflecting the deteriorated crystallinity of codoped ZnO thin films. We also tried to find the optimal composition in the tantalum and N codoped ZnO films to create a maximum excess carrier without crystal disruption. Ta, N-ZnO films with proper N doping concentration (i.e., 6 at.%) revealed the superior crystallinity and less structural defects, which can profit carrier lifetime and lead to an advantage of conductivity. Moreover, it was found that 2 at.% Ta and 6 at.% N codoped ZnO thin film have a high level of transmittance (>98%) in the visible region with the lowest resistivity of the order of $9.70 \times 10^{-5}$ $\Omega$ cm. As a result, the experimental FE characteristics exhibit that the tantalum and N codoped film device with N doping concentration of 6 at.% presented the optimum FE characteristics in this work (i.e., the higher current density of 1.33 mA $cm^{-2}$, larger field-enhancement factor ($\beta$) of ~4706 $\pm$ 3, lower turn-on field of 2.6 V $\mu m^{-1}$, and lower threshold field of 3.5 V $\mu m^{-1}$), attributed to the superior crystallinity, less structural defects, and better conductivity. In conclusion, the atmospheric pressure-based electrospraying method has been employed to fabricate the tantalum and N codoped ZnO thin films with superior electrical, optical, and field-emission characteristics and

has potential applications as both an excellent transparent electrode and field-emission devices.

## AUTHOR INFORMATION

### Corresponding Author

*Tel.: +82-42-350-3298. Fax: +82-42-350-3910. E-mail: SeungBinPark@kaist.ac.kr.

### Notes

The authors declare no competing financial interest.

## ACKNOWLEDGMENTS

This work was supported by the 2010 Research Fund by the Korea government.

## REFERENCES

(1) Hwang, K. S.; Jeong, J. H.; Jeon, Y. S.; Jeon, K. K.; Kim, B. H. *Ceram. Int.* **2007**, *33*, 505−507.
(2) Yan, X.; Tay, B. K.; Miele, P. *Carbon* **2008**, *46*, 753.
(3) Fancher, C. A.; De Clera, H. L.; Thomas, O. C.; Robinson, O. W.; Bowen, K. H. *J. Chem. Phys.* **1998**, *109*, 8426.
(4) Lee, J. H.; Park, B. Ok. *Thin Solid Films* **2003**, *426*, 94.
(5) Jin, Y.; Wang, J.; Sun, B.; Blakesley, J. C.; Greenham, N. C. *Nano Lett.* **2008**, *8*, 1649.
(6) Soci, C.; Zhang, A.; Xiang, B.; Dayeh, S. A.; Aplin, D. P. R.; Park, J.; Bao, X. Y.; Lo, Y. H.; Wang, D. *Nano Lett.* **2007**, *7*, 1003.
(7) Wang, R.; Sleight, A. W.; Cleary, D. *Chem. Mater.* **1996**, *8*, 433.
(8) Ambrosini, A.; Malo, S.; Poeppelmeier, K. *Chem. Mater.* **2002**, *14*, 58.
(9) Palmer, G. B.; Poeppelmeier, K. R.; Mason, T. O. *Chem. Mater.* **1997**, *9*, 3121.
(10) Zhang, S. B.; Wei, S. H.; Zunger, A. *Phys. Rev. B* **2001**, *63*, 075205.
(11) Look, D. C.; Reynolds, D. C.; Litton, C. W.; Jones, R. L.; Eason, D. B.; Cantwell, G. *Appl. Phys. Lett.* **2002**, *81*, 1830.
(12) Ryu, Y. R.; Zhu, S.; Look, D. C.; Wrobel, J. M.; Jeong, H. M.; White, H. W. *J. Cryst. Growth* **2000**, *216*, 330.
(13) Du, G. T.; Ma, Y.; Zhang, Y. T.; Yang, T. P. *Appl. Phys. Lett.* **2005**, *87*, 213103.
(14) Sanmya, M.; Tomita, Y.; Kobayashi, K. *Chem. Mater.* **2003**, *15*, 819.
(15) Bian, J. M.; Li, X. M.; Gao, X. D.; Yu, W. D.; Chen, L. D. *Appl. Phys. Lett.* **2004**, *84*, 541.
(16) Yuan, G. D.; Ye, Z. Z.; Zhu, L. P.; Qian, Q.; Zhao, B. H.; Fan, R. X.; Perkins, C. L.; Zhang, S. B. *Appl. Phys. Lett.* **2005**, *86*, 202106.
(17) Joeph, M.; Tabata, H.; Saeki, H.; Ueda, K.; Kawai, T. *Phys. B* **2001**, *302/ 303*, 140.
(18) Mahmood, K.; Song, D. S.; Park, S. B. *Surf. Coat. Technol.* **2012**, *206*, 4730−4740.
(19) Hu, J.; Gordon, R. G. *Solar Cell* **1991**, *30*, 437.
(20) Robbins, J. J.; Harvey, J.; Leaf, J.; Fry, C.; Wolden, C. A. *Thin Solid Films* **2005**, *473*, 35.
(21) Shan, F. K.; Shin, B. C.; Jang, S. W.; Yu, Y. S. *J. Eur. Ceram. Soc.* **2004**, *24*, 1015.
(22) Chaabouni, F.; Abaab, M.; Rezig, B. *Mater. Sci. Eng., B* **2004**, *109*, 236.
(23) Paraguay, F. D.; Yoshida, M. M.; Morales, J.; Solis, J.; Estrada, W. L. *Thin Solid Films* **2000**, *373*, 137.
(24) Mahmood, K.; Park, S. B. *J. Mater. Chem. A* **2013**, *1*, 4826−4835.
(25) Powder Diffraction Files, Joint Committee on Powder Diffraction Standards; ASTM: Philadelphia, PA, 1967, Card 36−1451.
(26) Lu, Y. M.; Hwang, W. S.; Liu, W. Y.; Yang, J. S. *Mater. Chem. Phys.* **2001**, *72*, 269.
(27) Lee, J. H.; Ko, K. H.; Park, B. O. *J. Cryst. Growth* **2003**, *247*, 119.
(28) http://en.wikipedia.org/wiki/Ionic radius. (Accessed January 20, 2013).
(29) Deng, H.; Russell, J. J.; Lamb, R. N.; Jiang, B.; Li, Y.; Zhou, X. Y. *Thin Solid Films* **2004**, *458*, 43.
(30) Wang, X. B.; Song, C.; Geng, K. W.; Zeng, F.; Pan, F. *J. Phys. D: Appl. Phys.* **2006**, *39*, 4992.
(31) Hu, J.; Gordon, R. G. *J. Appl. Phys.* **1992**, *72*, 5381.
(32) Nunes, P.; Fortunato, E.; Tonello, P.; Fernandes, F. B.; Vilarinho, P.; Martins, R. *Vacuum* **2002**, *64*, 281.
(33) Manounia, A. El.; Manjónb, F. J.; Mollar, M.; Maríb, B.; Gómez, R.; López, M. C.; Barradod, J. R. R. *Superlattices Microstruct.* **2006**, *39*, 185−192.
(34) Zhou, H. M.; Yi, D. Q.; Yu, Z. M.; Xiao, L. R.; Li, J. *Thin Solid Films* **2007**, *515*, 6909−6914.
(35) Kim, G. H.; Bang, J. G.; Kim, Y. S.; Rout, S. K.; Woo, S. I. *Appl. Phys. A: Mater. Sci. Process.* **2009**, *97*, 821.
(36) Kim, G. H.; Hwang, D. H.; Woo, S. I. *Mater. Chem. Phys.* **2011**, *131*, 77−83.
(37) Chen, M., Cullity, B. D. *Elements of X-ray Diffractions*; Addison-Wesley: Reading, MA, 1978; p 102.
(38) Lide, D. R., Ed. *Chemical Rubber Company Handbook of Chemistry and Physics*, 81st ed.; CRC Press: Boca Raton, FL, 2000.
(39) Atanassova, E.; Dimitrova, T.; Koprinarova, J. *Appl. Surf. Sci.* **1995**, *84*, 193.
(40) Joseph, B.; Manoj, P. K.; Vaidyan, V. K. *Ceram. Int.* **2006**, *32*, 487−493.
(41) Bursten, E. *Phys. Rev.* **1954**, *93*, 632.
(42) Gao, L.; Zhang, Y.; Zhang, J. M.; Xu, K. W. *Appl. Surf. Sci.* **2011**, *257*, 2498−2502.
(43) Abrarov, S. M.; Yuldashev, Sh. U.; Kim, T. W.; Kwon, Y. H.; Kang, T. W. *Opt. Commun.* **2006**, *259*, 378−384.
(44) Marotti, R. E.; Giorgi, P.; Machado, G.; Dalchiele, E. A. *Sol. Energy Mater. Sol. Cells* **2006**, *90*, 2356.
(45) Lin, S. S.; Huang, J. L. *Surf. Coat. Technol.* **2004**, *185*, 222.
(46) Minami, T. *Semicond. Sci. Technol.* **2005**, *20*, S35.
(47) Muiva, C. M.; Sathiaraj, T. S.; Maabong, K. *Ceram. Int.* **2011**, *37*, 555−560.
(48) Kim, S. M.; Rim, Y. S.; Keum, M. J.; Kim, K. H. *J. Electroceram.* **2009**, *23*, 341−345.
(49) Hu, J.; Gordon, R. G. *Mater. Res. Soc. Symp. Proc.* **1992**, *242*, 743.
(50) Fowler, R. H.; Nordheim, L. W. *Proc. R. Soc. London, Ser. A* **1928**, *119*, 173.
(51) Jo, S. H.; Banerjee, D.; Ren, Z. F. *Appl. Phys. Lett.* **2004**, *85*, 1407.
(52) Zhu, Y. W.; Zhang, H. Z.; Sun, X. C.; Feng, S. Q.; Xu, J.; Zhao, Q.; Xiang, B.; Wang, R. M.; Yu, D. P. *Appl. Phys. Lett.* **2003**, *83*, 144−146.
(53) Zhao, Q.; Zhang, H. Z.; Zhu, Y. W.; Feng, S. Q.; Sun, X. C.; Xu, J.; Yu, D. P. *Appl. Phys. Lett.* **2005**, *86*, 203115−203117.
(54) Hao, X. T.; Ma, J.; Zhang, D. H.; Yang, T. L.; Ma, H. L.; Yang, Y. G.; Cheng, C. F.; Huang, J. *Appl. Surf. Sci.* **2001**, *183*, 137.
(55) Kim, H.; Horwitz, J. S.; Kushto, G.; Piqué, A.; Kafafi, Z. H.; Gilmore, C. M.; Chrisey, D. B. *J. Appl. Phys.* **2000**, *88*, 6021.
(56) Xue, X. Y.; Li, L. M.; Yu, H. C.; Chen, Y. J.; Wang, Y. G.; Wang, T. H. *Appl. Phys. Lett.* **2006**, *89*, 043118.